electronic materials

MDPI

Communication

Size-Controlled ZnO Nanoparticles Synthesized with Thioacetamide and Formation of ZnS Quantum Dots

Ju-Seong Kim, Jonghyun Choi and Won Kook Choi *

Center for Opto-Electronic Materials and Devices, Korea Institute of Science and Technology (KIST), Seoul 02792, Republic of Korea; jskim5772@kist.re.kr (J.-S.K.); jhchoi325@korea.ac.kr (J.C.)
* Correspondence: wkchoi@kist.re.kr; Tel.: +82-2-958-5562

Abstract: In this work, we report the first attempt to investigate the dependence of thioacetamide (TAA) on the size of ZnO nanoparticles (NPs) in forming ZnS nanostructures from ZnO. Size-controlled B(blue)_, G(green)_, and Y(yellow)_ZnO quantum dots (QDs) and NC (nanocrystalline)_ZnO NPs were synthesized using a sol–gel process and a hydrothermal method, respectively, and then reacted with an ethanolic TAA solution as a sulfur source. ZnO QDs/NPs began to decompose into ZnS QDs through a reaction with TAA for 5~10 min, so rather than forming a composite of ZnO/ZnS, ZnO QDs and ZnS QDs were separated and remained in a mixed state. At last, ZnO QDs/NPs were completely decomposed into ZnS QDs after a reaction with TAA for 1 h irrespective of the size of ZnO QDs up to ~50 nm. All results indicate that ZnS formation is due to direct crystal growth and/or the chemical conversion of ZnO to ZnS.

Keywords: size-controlled ZnO nanoparticles; the formation of ZnS nanoparticles; quantum dots; sol–gel; hydrothermal; ethanolic thioactamide; crystal growth; chemical conversion

check for updates

Citation: Kim, J.-S.; Choi, J.; Choi, W.K. Size-Controlled ZnO Nanoparticles Synthesized with Thioacetamide and Formation of ZnS Quantum Dots. *Electron. Mater.* **2023**, *4*, 139–147. https://doi.org/10.3390/electronicmat4040012

Academic Editor: Wojciech Pisula

Received: 5 September 2023
Revised: 29 September 2023
Accepted: 10 October 2023
Published: 12 October 2023

1. Introduction

II-VI ZnO semiconductors have received considerable attention because of their advantages, such as a wide band gap (3.37 eV), large exciton binding energy (60 meV), high electron mobility (≈205 cm^2/Vs), high optical transparency, low toxicity in vivo, and low price due to the abundance of resources [1–11]. Specifically, ZnO quantum dots (QDs) are a promising material due to their advantages, such as a size-tunable band gap and electrical properties, and they do not require altering the composition and have a low-cost fabrication technique that is compatible with solution-processed methods [12–16]. Therefore, ZnO QDs have been most widely adopted as an electron transport layer (ETL) in photovoltaic cells, light-emitting diodes, and photocatalysts [17–23]. Despite these many advantages, however, ZnO QDs have difficulty controlling excessive trap levels and structural luminescence weakness, in which a direct band edge (band-to-band) emission is rapidly reduced due to surface defects [24,25]. Several studies have demonstrated ways to improve the intrinsic properties of ZnO, including the control and design of the point defect structures as well as surface and interfacial structures [26–31]. More specifically, using ZnO/ZnS nanocomposites is an attractive approach to modifying the particle characteristics and properties of ZnO [32,33]. ZnO/ZnS nanocomposites, such as core–shell QDs, nanorods, nanowires, nanobelts, and nanocages, have been successfully prepared using various methods [34–43]. Herein, the shell can act as a barrier between the shell interior and the surrounding environment, eliminate surface-related defect states, and improve physical and chemical stability. In addition, the photoluminescence properties of the core can be improved by reducing the non-radiative recombination of photogenerated electron–hole pairs [44]. In forming ZnO/ZnS nanostructures, Na_2S and thioacetamide (TAA) are commonly used as sulfur sources, whereas few results have been reported for nanocomposites using TAA on ZnO NPs. For example, Luo et al. reported Cd-doped ZnO/ZnS core/shell QDs and obtained ZnO/ZnS core/shell QDs with significantly reduced visible emissions using

TAA [33]. Manaia et al. also obtained ZnO/ZnS heterostructures prepared with different concentrations of the sulfur source (TAA) [45]. As these results regarding TAA-induced ZnS formation have not been clearly interpreted, a special approach is required to better understand them.

In this work, we first attempted to use size-controlled ZnO NPs to analyze the role of TAA in the formation of ZnS nanostructures from ZnO. We prepared samples of small-sized Y_, G_, and B_ZnO QDs, named according to their PL wavelengths, blue, green, and yellow, and a sample of NC (nanocrystalline)_ZnO NPs a few tens of nanometers in size. The B_, G_, and Y_ZnO QDs samples were synthesized at low temperatures via a simple sol–gel method, as described in our previous reports [46]. The NC_ZnO NPs were synthesized through a hydrothermal method using a zinc acetate dihydrate (ZAD) precursor solution [47]. The size-controlled B_, G_, and Y_ZnO QDs and NC_ZnO NPs were reacted with the same amount of TAA solution and analyzed according to the reaction progress time. The crystalline structure and crystallite size of nanocomposites were characterized via X-ray diffraction (XRD) and a transmission electron microscope (TEM). UV-vis spectroscopy, photoluminescence (PL), and photoluminescence excitation (PLE) were adopted to further estimate the average particle size and to analyze the optical properties of ZnO synthesized with/without TAA. During the reaction of all size-controlled ZnO NPs with TAA, the ZnO NPs were completely consumed and ZnS QDs were newly formed, regardless of the size of ZnO NPs. Our results enable a broader understanding of the synthetic mechanisms involved in the use of TAA as a sulfur source in forming ZnS QDs using ZnO QDs/NPs.

2. Materials and Methods

2.1. Materials

Zinc acetate dihydrate (ZAD, 99.0%), lithium hydroxide (LiOH, 98.0%), N, N-Dimethy lformamide (DMF, 99.9%), thioacetamide (TAA, 99%), n-hexane, and anhydrous ethanol (EtOH) were purchased from Sigma Aldrich and used without any further purification.

2.2. Synthesis of ZnO NPs

All size-controlled ZnO NPs were prepared using a previously reported similar method with modifications. The ZnO QDs were synthesized at low temperatures via a simple sol–gel method [46]. Solutions of ZAD and LiOH were prepared in EtOH and stirred at 60 °C for 1 day. The LiOH solution was added dropwise to the ZAD solution in a 250 mL flask at 70 °C and stirred for 1 h. In order to synthesize B_, G_, and Y_ZnO, LiOH/ZAD solutions with molar ratios of 1.2, 1.6, and 2.16, respectively, were used. The NC_ZnO NPs were synthesized through a hydrothermal method using a ZAD solution [42]. A total of 0.92 g of ZAD prepared in 200 mL of DMF was stirred at 110 °C for 5 h. Then, the resulting solutions were separated via centrifugation. Finally, the ZnO NPs were obtained by repeating the two-step purification process with n-hexane and drying.

2.3. Synthesis of ZnS QDs with TAA and ZnO NPs

The ZnS QDs were prepared using previously reported similar methods with modifications [33,45]. Both 1.317 g of ZAD and 0.3 g of TAA were dissolved in EtOH and stirred at 40 °C until fully dissolved. A given amount of the solution and an equal volume of the ZnO solutions were mixed at room temperature under constant stirring. The TAA solution was added to the ZAD solution and B_, G_, and Y_ZnO QDs and NC_ZnO NPs at 40 °C and stirred for 1 h. The solutions were repeatedly washed with n-hexane to remove the residue.

2.4. Characterization

The X-ray diffraction (XRD) patterns of the samples were recorded using an X-ray diffractometer (Rigaku ATX-G, The Woodlands, TX, USA) with Cu Kα radiation at the wavelength λ = 1.5406 Å. Using a transmission electron microscope (TEM, TalosF200X), the morphology, size, and elemental composition of the samples were investigated. TEM

samples were prepared by dispersing ZnO dry powders in deionized water or EtOH to form a homogeneous suspension. The size distribution of ZnO samples was analyzed using TEM imaging and analysis software (Tecnai 3.0, FEI Co., Ltd., Kanagawa, Japan). UV-Vis absorption data were recorded with a PerkinElmer Lambda 18 UV–vis spectrometer with QS-grade quartz cuvettes. PL and PLE data were recorded with a Hitachi F-7000 fluorescence system with QS-grade quartz cuvettes.

3. Results and Discussion

The chemical reaction of ZnO NPs and ZnS QDs is presented in Scheme 1. After base-catalyzed hydrolysis and condensation reactions from ZAD precursors to ZnO particles, as shown in reaction (1) [48–50], the TAA solution used as a sulfur source was added to the size-controlled ZnO NPs, as shown in reaction (2) [51,52]. TAA, when used as a sulfur source, can induce the conversion of ZnO to ZnS through multiple complex chemical reactions. When acetate moieties in ethanolic ZAD solutions are released, acetic acid, esters, or additional water can be formed through a reaction with ethanol. TAA can be decomposed by water formed from ZAD, releasing acetamide and S ions. Here, with a sufficient amount of TAA, full chemical conversion of ZnO to ZnS could be expected according to their respective solubility constants [33,45,48,53].

$$\underset{ZAD}{ZnAc_2 \cdot 2H_2O} \xrightarrow[\triangle]{} AcO-Zn-OAc \xrightarrow{OH^-} HO-Zn-OH + HO-Zn-OH$$

$$\longrightarrow HO-Zn-O-Zn-OH \longrightarrow ZnO_{(s)} \qquad (1)$$

$$\underset{TAA}{CH_3CSNH_2} + H_2O \longrightarrow CH_3CONH_2 + H_2S$$

$$Zn^{2+} + H_2S \longrightarrow ZnS_{(s)} + 2H^+ \qquad (2)$$

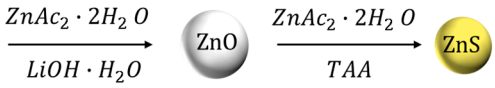

Scheme 1. Schematic illustration of the synthesis of ZnO and ZnS QDs.

Figure 1 presents the XRD patterns of ZnO samples synthesized without TAA and with TAA for 1 h. ZnO had a hexagonal wurtzite structure with diffraction peaks of (100), (002), (101), (102), (110), (103), and (112) crystalline planes and ZnS had a cubic zinc blende structure with diffraction peaks of (111), (220), and (311) crystalline planes. The positions of the XRD patterns of ZnO are marked with dashed black lines, while those indicative of ZnS are marked with dashed red lines. The absence of impurity peaks was expected because of the high purity of the sample. Here, all diffraction peaks of the ZnO samples synthesized without TAA are in good agreement with those of hexagonal wurtzite ZnO (PDF No. 36-1451). The narrowing of peaks in the diffraction patterns of all the synthesized products clearly indicates the formation of big-sized NCs from small-sized QDs. In the case of the NC_ZnO NPs, which show relatively clear-grain crystal characteristics, the average size of particles could be estimated using the Debye–Scherrer equation, and the crystallite size was about 45 nm [54]. On the other hand, all diffraction peaks of the ZnO samples synthesized with TAA are consistent with the ZnS phase (PDF No. 05-0566). For the ZnO NPs synthesized with TAA for 1 h, the remarkable XRD patterns of ZnO were not identified. These results indicate that wurtzite ZnO particles synthesized with TAA can be consumed and the cubic zinc blende ZnS formed.

TEM images of the ZnO samples synthesized without TAA and the ZnO samples synthesized with TAA are presented in Figure 2. As is apparent from Figure 2(top), B_, G, and Y_ZnO QDs synthesized without TAA presented approximately spherical shapes with an approximate diameter of about 2.6, 2.9, and 3.2 nm, respectively. It is noteworthy that G_ and Y_ZnO QDs were well dispersed, whereas the B_ZnO QDs agglomerated because of their high surface energy. The NC_ZnO NPs synthesized without TAA presented

approximately distorted hexagonal shapes with an approximate diameter of more than 40 nm, which agrees well with the value of about 45 nm calculated using the Debye–Scherrer equation in XRD. On the other hand, the B_, G_, and Y_ZnO QDs and NC_ZnO NPs synthesized with TAA finally vanished, and only spherical ZnS QDs with similar diameters of 2.2 nm were observed in all samples, as shown in Figure 2(bottom). Here, the NC_ZnO NP with the largest diameter was consumed without a trace, as shown in Figure 2(inset in the white square). This can be interpreted as the consumption of ZnO regardless of the particle size with the simultaneous formation of ZnS QDs and is in good agreement with our XRD results.

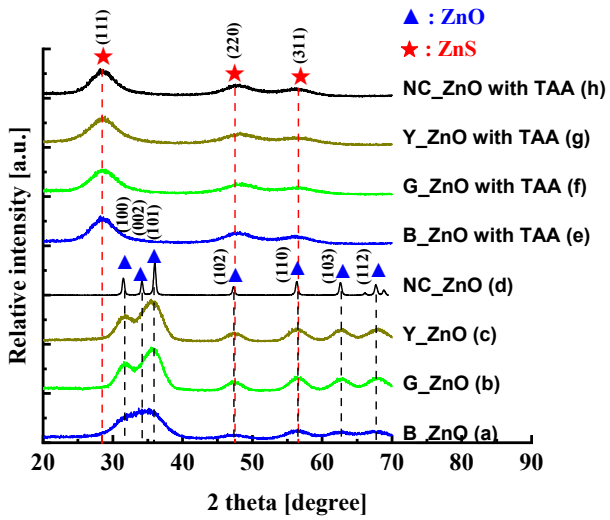

Figure 1. XRD patterns for (**a**) B_ZnO QDs, (**b**) G_ZnO QDs, (**c**) Y_ZnO QDs, and (**d**) NC_ZnO NPs and ZnO QDs without TAA and those with TAA (**e**–**h**).

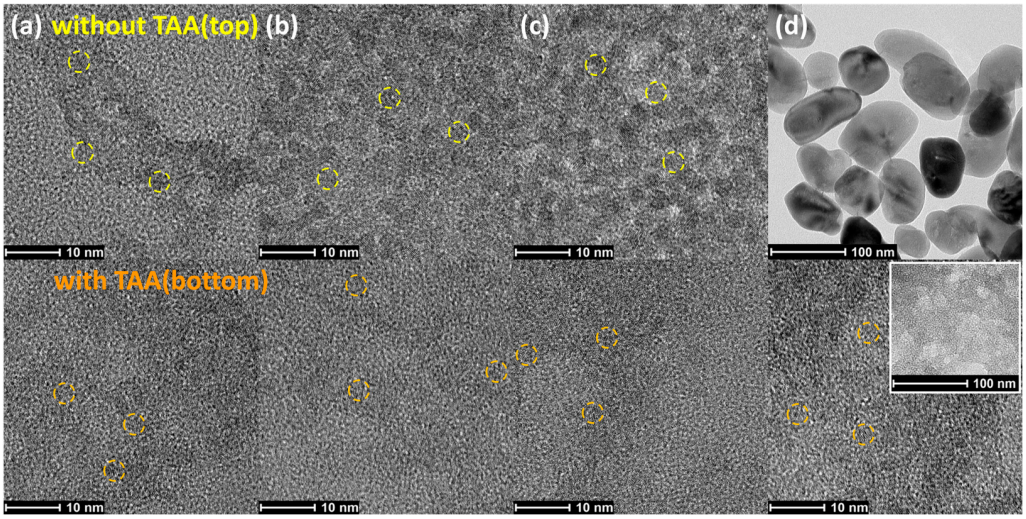

Figure 2. TEM images for ZnO synthesized without TAA (**top**) and with TAA (**bottom**). (**a**) B_ZnO QDs, (**b**) G_ZnO QDs, (**c**) Y_ZnO QDs, and (**d**) NC_ZnOs (inset shows low magnification of TEM images).

UV-Vis absorption spectra of different reaction times with/without TAA are presented in Figure 3. With decreasing particle size, a blue shift of excitonic absorption and an increase in band gap are known to occur for QDs. In the absorption spectra, differences in the particle size of B_, G_, Y_, and NC_ZnOs are clearly observed. The B_, G_, and Y_ZnO QDs and NC_ZnO NPs synthesized without TAA exhibited absorption peaks at 297, 322, 333, and 370 nm, respectively. According to the equation reported by Meulenkamp [55],

the particle sizes of the ZnO QDs but not NC_ZnO NPs could be estimated at the measured absorption wavelengths of 2.6, 3.2, and 3.5 nm for B_, G_, and Y_ZnO QDs, respectively, which is consistent with the results measured with the TEM. No dramatic change in ZnO particle size was observed as the reaction with TAA proceeded. In the absorption spectra of B_ZnO QDs, after synthesis for 5 min with TAA, a new absorption peak appeared at 266 nm, being different from the peak at 322 nm that appeared for ZnO, which indicates that the new material was formed. And then the peak at 322 nm completely disappeared after synthesis for 10 min with TAA and a new broad peak at around 290 nm additionally appeared, which indicates that the ZnO NPs were almost entirely consumed. This results from the use of ZnO as a zinc source when forming ZnS QDs. The excitonic peaks at about 266 nm and 290 nm are well-known characteristic peaks of ZnS QDs [45,56–58]. Therefore, it is believed that ZnO and ZnS QDs co-existed in the B_ZnO QDs after synthesis for 5 min with TAA. The absorption spectra for both Y_ZnO and G_ZnO QDs show similar behavior to those of B_ZnO QDs. In the case of NC_ZnO NPs, after synthesis with TAA, the absorption peak at 290 nm, instead of that at 266 nm, was more dominantly observed. From the above results, it can be suggested that the absorption peaks of B_, G_, and Y_ZnO QDs and NC_ZnO NPs related to ZnO rapidly decrease 5 to 10 min into a reaction with TAA and finally vanish as the reaction proceeds. On the other hand, the absorption peaks of ZnS QDs at 266 (Figure 3a–c) and 290 nm (Figure 3d) remained clear as the reaction proceeded. This can be interpreted as the consumption of ZnO regardless of the particle size with the simultaneous formation of ZnS QDs.

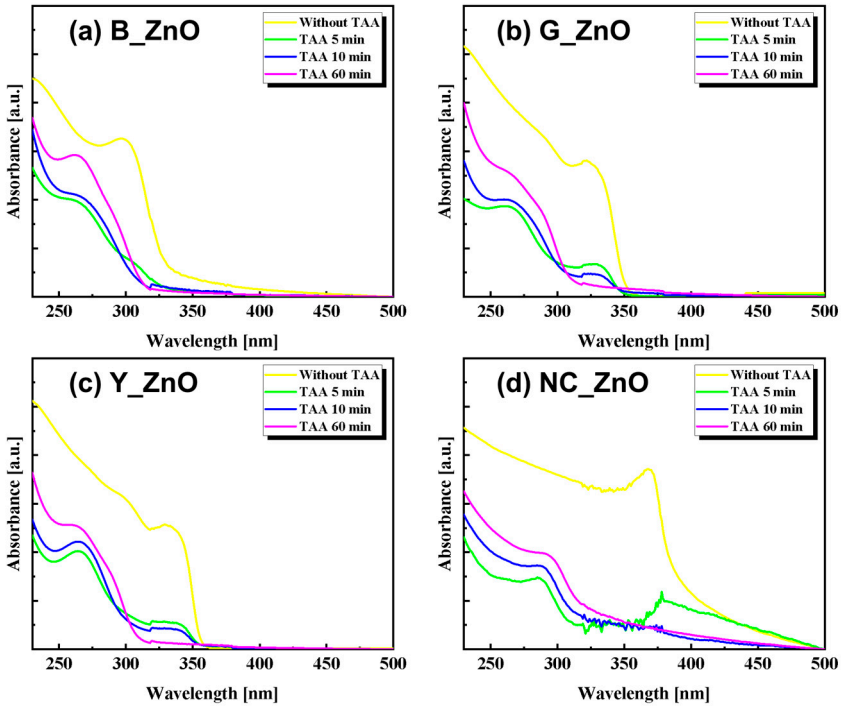

Figure 3. UV-Vis absorption spectra of size-controlled ZnO NPs synthesized with/without TAA measured at the indicated reaction times. (**a**) B_ZnO, (**b**) G_ZnO, (**c**) Y_ZnO QDs, and (**d**) NC_ZnO NPs.

The PL spectra of ZnO NPs synthesized for different reaction times with/without TAA are presented in Figure 4. For the optical mechanisms underlying the PL of ZnO NPs synthesized without TAA, the visible-light emission is due to trap-induced defects on the surface, and UV luminescence corresponds to band-to-band emission [24,25]. The B_, G_, and Y_ZnO QDs and NC_ZnO NPs exhibited PL peaks centered at 466, 528, 538, and 378 nm, respectively. These PL results for B_, G_, and Y_ZnO QDs are in good agreement with the occurrence of a blue shift of the PL wavelength as the particle size decreased. After reacting with TAA for 5 min, the PL peaks of ZnO QDs gradually disappeared, but

a new peak around 420 nm appeared clearly in all the samples. The PL peak at about 420 nm is a well-known characteristic of ZnS QDs [45,53,56–58]. In addition, the PL peak characteristic of visible luminescence corresponding to ZnO was significantly decreased for B_ZnO QDs, moderately decreased for G_ and Y_ZnO QDs, and slightly decreased for NC_ZnO. The PL peak characteristic of relatively small-sized B_ZnO QDs disappeared faster than that of other G_ and Y_ZnO QDs, which is likely due to the rapid consumption of smaller particles. In general, in most core/shell QDs, the PL property of the inner QDs can be improved with the shell of other materials, which reduces the dangling bonds or structural defects distributed at the surface. In our case, the expected enhancement of the excitonic emission in ZnO NPs with the suppression of visible luminescence could not be seen with the increase in reaction time with TAA, but the improved PL intensity of ZnS QDs was clearly seen. After reacting with TAA for 60 min, only the PL peak characteristic of ZnS was observed in all the samples. This indicates that the reaction of ZnO NPs with TAA resulted in the formation of ZnS QDs rather than the surface shell effect of ZnO NPs.

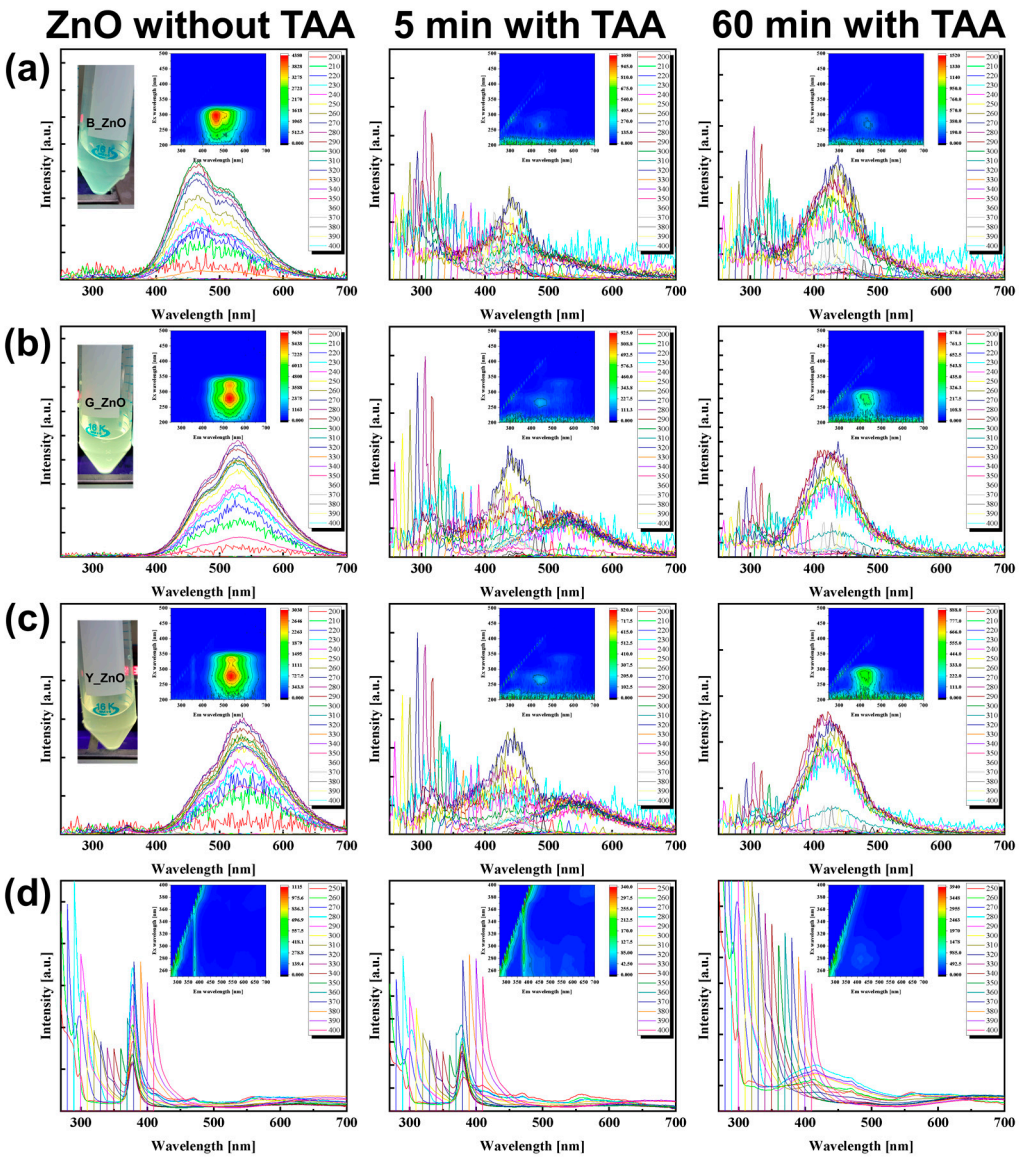

Figure 4. PL characteristics of size-controlled ZnO NPs synthesized with/without TAA measured at the indicated reaction times; inset shows excitation and emission map for PL (left: without TAA, inset pictures show the luminescent images of ZnO NPs under UV excitation at 365 nm; middle: synthesized for 5 min with TAA; right: synthesized for 60 min with TAA). (**a**) B_ZnO QDs, (**b**) G_ZnO QDs, (**c**) Y_ZnO QDs, and (**d**) NC_ZnO NPs.

According to the experimental results described above, we propose a possible mechanism by which ZnS QDs are formed from ZnO NPs. S^{2-} released from the decomposition of TAA reacts with Zn^{2+} slowly dissolved from the surface of ZnO to produce ZnS QDs around the ZnO NPs. A non-uniform shell composed of ZnS QDs is gradually formed surrounding the ZnO NPs. As the sulfidation time increases, Zn^{2+} ions diffuse outward towards the shell, whereas the S^{2-} ions diffuse inwards towards the core. Such an effect is a consequence of the difference in the concentration gradient of Zn^{2+} and S^{2-} ions in the solution, as suggested by the Kirkendall effect [51,52]. Therefore, the simultaneous occurrence of both a decrease in the size of the ZnO core and the growth of ZnS is in good agreement with our results. Likewise, in the case of NC_ZnO NPs, despite having the largest size, no characteristics of residual ZnO were observed after the reaction with TAA. This results from the use of ZnO NPs as a source of zinc in the formation of ZnS QDs. Depending on the solubility constant, a sufficient amount of TAA can result in complete chemical conversion from ZnO with a less than 50 nm diameter to ZnS QDs.

4. Conclusions

Size-controlled Y_, G_, and B_ZnO QDs synthesized using a sol–gel method and a NC_ZnO NPs a few tens of nanometers in size synthesized using the hydrothermal method were reacted with TAA as a sulfur source to synthesize ZnO/ZnS core–shell structures. ZnO QDs/NPs were completely decomposed into ZnS QDs after a reaction with TAA for 1 h irrespective of the size of ZnO QDs up to ~50 nm without forming any intermediate ZnO/ZnS composites. All results indicate that ZnS formation is due to direct crystal growth and/or the chemical conversion of ZnO to ZnS through the chemical reaction of S^{2-} released from the decomposition of TAA with Zn^{2+} slowly dissolving from the surface of ZnO. Our results enable a broader understanding of the synthetic mechanisms involved in the use of TAA as a sulfur source in forming ZnS QDs from ZnO QDs/NPs.

Author Contributions: J.-S.K. performed the experiment and analysis. J.C. provided the NC_ZnO NPs synthesized without TAA. J.C. and W.K.C. advised on the project, and J.-S.K. and W.K.C. wrote this manuscript. All authors have read and agreed to the published version of the manuscript.

Funding: This work was supported by the NRF (National Research Foundation of Korea) grant funded by the Korean Government (NRF-2021-Global Ph.D. Fellowship Program) and the KIST Institutional Program (2E32242, 2V09706).

Data Availability Statement: No new data were created or analyzed in this study. Data sharing does not apply to this article.

Conflicts of Interest: The authors declare no conflict of interest.

References

1. Morkoç, H.; Özgür, Ü. *Zinc Oxide*; Wiley-VCH Velag GmbH & Co. KGaA: Weinheim, Germany, 2009.
2. Furno, E.; Bertazzi, F.; Goano, M.; Ghione, G.; Bellotti, E. Hydrodynamic transport parameters of wurtzite ZnO from analytic- and full-band Monte Carlo simulation. *Solid-State Electron.* **2008**, *52*, 1796. [CrossRef]
3. Park, J.-S.; Kyhm, J.; Kim, H.H.; Jeong, S.; Kang, J.; Lee, S.-E.; Lee, K.-T.; Park, K.; Barange, N.; Han, J.; et al. Alternative Patterning Process for Realization of Large-Area, Full-Color, Active Quantum Dot Display. *Nano Lett.* **2016**, *16*, 6946. [CrossRef]
4. Chao, M.-R.; Chang, Y.-Z.; Chen, J.-L. Hydrophilic ionic liquid-passivated CdTe quantum dots for mercury iondetection. *Biosens. Bioelectron.* **2013**, *42*, 397–402. [CrossRef]
5. Tan, L.; Kang, C.; Xu, S.; Tang, Y. Selective room temperature phosphorescence sensing of target protein using Mn-doped ZnS QDs-embedded molecularly imprinted polymer. *Biosens. Bioelectron.* **2013**, *48*, 216–223. [CrossRef] [PubMed]
6. Zou, W.-S.; Qiao, J.-Q.; Hu, X.; Ge, X.; Lian, H.-Z. Synthesis in aqueous solution and characterisation of a new cobalt-doped ZnS quantum dot as a hybrid ratiometric chemosensor. *Anal. Chim. Acta* **2011**, *708*, 134–140. [CrossRef] [PubMed]
7. Liu, J.; Wei, X.; Qu, Y.; Cao, J.; Chen, C.; Jiang, H. Aqueous synthesis and bio-imaging application of highly luminescent and low cytotoxicity Mn^{2+}-doped ZnSe nanocrystals. *Mater. Lett.* **2011**, *65*, 2139–2141. [CrossRef]
8. Subash, B.; Krishnakumar, B.; Pandiyan, V.; Swaminathan, M.; Shanthi, M. An efficient nanostructured Ag_2S–ZnO for degradation of Acid Black 1 dye under day light illumination. *Sep. Purif. Technol.* **2012**, *96*, 204–213. [CrossRef]
9. Liu, C.; Wang, Y.; Meng, D.; Yu, X.; Wang, Y.; Liu, J.; Lu, C.; Xu, K. Enhanced visible light photocatalytic performance of ZnO/ZnS/CuS ternary nanocomposites. *Mater. Lett.* **2014**, *122*, 197–200. [CrossRef]

10. Nguyen, H.T.; Nguyen, N.D.; Lee, S. Application of solution-processed metal oxide layers as charge transport layers for CdSe/ZnS quantum-dot LEDs. *Nanotechnology* **2013**, *24*, 115201. [CrossRef] [PubMed]
11. Janotti, A.; Walle, C.G. Van de, Fundamentals of zinc oxide as a semiconductor. *Rep. Prog. Phys.* **2009**, *72*, 126501. [CrossRef]
12. Xiong, H.-M. ZnO Nanoparticles Applied to Bioimaging and Drug Delivery. *Adv. Mater.* **2013**, *37*, 5329–5335. [CrossRef] [PubMed]
13. Matsuyama, K.; Ihsan, N.; Irie, K.; Mishima, K.; Okuyamam, T.; Mutom, H. Bioimaging application of highly luminescent silica-coated ZnO-nanoparticle quantum dots with biotin. *J. Colloid Interface Sci.* **2013**, *399*, 19–25. [CrossRef]
14. Moussodia, R.-O.; Balan, L.; Merlin, C.; Mustin, C.; Schneider, R. Biocompatible and stable ZnO quantum dots generated by functionalization with siloxane-core PAMAM dendrons. *J. Mater. Chem.* **2010**, *20*, 1147–1155. [CrossRef]
15. Manaia, E.B.; Kaminski, R.C.K.; Caetano, B.L.; Briois, V.; Chiavacci, L.A.; Bourgaux, C. Surface modified Mg-doped ZnO QDs for biological imaging. *Eur. J. Nanomed.* **2015**, *7*, 109–120. [CrossRef]
16. Zhao, H.; Lv, P.; Huo, D.; Zhang, C.; Ding, Y.; Xu, P.; Hu, Y. Doxorubicin loaded chitosan-ZnO hybrid nanospheres combining cell imaging and cancer therapy. *RSC Adv.* **2015**, *5*, 60549–60551. [CrossRef]
17. Xu, B.; Gopalan, S.-A.; Gopalan, A.-I.; Muthuchamy, N.; Lee, K.-P.; Lee, J.-S.; Jiang, Y.; Lee, S.-W.; Kim, S.-W.; Kim, J.-S.; et al. Functional solid additive modified PEDOT:PSS as an anode buffer layer for enhanced photovoltaic performance and stability in polymer solar cells. *Sci. Rep.* **2017**, *7*, 45079. [CrossRef]
18. Xu, B.; Gopalan, S.-A.; Jeong, H.-M.; Kim, S.-W.; Kim, J.-S.; Kwon, J.-B.; Kang, S.-W. Improving Air-Stability and Performance of Bulk Heterojunction Polymer Solar Cells Using Solvent Engineered Hole Selective Interlayer. *Materials* **2018**, *11*, 1143. [CrossRef]
19. Kim, J.-S.; Kim, S.-W.; Xu, B.; Kang, S.-W. High-Performance Quantum Dot-Light-Emitting Diodes with a Polyethylenimine Ethoxylated-Modified Emission layer. *Thin Solid Film* **2020**, *709*, 138179. [CrossRef]
20. Lee, Y.J.; Kim, H.H.; Lee, Y.J.; Kim, J.H.; Choi, H.-J.; Choi, W.K. Electron transport phenomena at the interface of Al electrode and heavily doped degenerate ZnO nanoparticles in quantum dot light emitting diode. *Nanotechnology* **2019**, *30*, 035207. [CrossRef]
21. Kim, H.H.; Kumi, D.O.; Kim, K.; Park, D.; Yi, Y.; Cho, S.H.; Park, C.; Ntwaeaborwa, O.M.; Choi, W.K. Optimization of the electron transport in quantum dot light-emitting diodes by codoping ZnO with gallium (Ga) and magnesium (Mg). *RSC Adv.* **2019**, *9*, 32066–32071. [CrossRef]
22. Mamiyev, Z.; Balayeva, N.O. Metal Sulfide Photocatalysts for Hydrogen Generation: A Review of Recent Advances. *Catalysts* **2022**, *12*, 1316. [CrossRef]
23. Mirzaeifard, Z.; Shariatinia, Z.; Jourshabani, M.; Darvishi, S.M.R. ZnO Photocatalyst Revisited: Effective Photocatalytic Degradation of Emerging Contaminants Using S-Doped ZnO Nanoparticles under Visible Light Radiation. *Ind. Eng. Chem. Res.* **2020**, *59*, 15894–15911. [CrossRef]
24. Ischenko, V.; Polarz, S.; Grote, D.; Stavarache, V.; Fink, K.; Driess, M. Zinc Oxide Nanoparticles with Defects. *Adv. Funct. Mater.* **2005**, *15*, 1945. [CrossRef]
25. Gong, Y.; Andelman, T.; Neumark, G.F.; O'Brien, S.; Kuskovsky, I.L. Origin of defect-related green emission from ZnO nanoparticles: Effect of surface modification. *Nanoscale Res. Lett.* **2007**, *2*, 297. [CrossRef]
26. Asok, A.; Gandhia, M.N.; Kulkarni, A.R. Enhanced visible photoluminescence in ZnO quantum dots by promotion of oxygen vacancy formation. *Nanoscale* **2012**, *4*, 4943–4946. [CrossRef]
27. Zhang, L.; Yin, L.; Wang, C.; Lun, N.; Qi, Y.; Xiang, D. Origin of Visible Photoluminescence of ZnO Quantum Dots: Defect-Dependent and Size-Dependent. *J. Phys. Chem. C* **2010**, *114*, 9651–9658. [CrossRef]
28. Kim, H.H.; Lee, H.; Kang, J.K.; Choi, W.K. Photoluminescence and Electron Paramagnetic Resonance Spectroscopy for Revealing Visible Emission of ZnO Quantum Dots. *Ann. Phys.* **2022**, *534*, 2100382. [CrossRef]
29. Kim, H.H.; Park, S.; Lee, H.; Kang, J.K.; Choi, W.K. Blue-Light Emissive Type II ZnO@ 5-Amino-2-Naphthalene Sulfonic Acid Core–Shell Quantum Dots. *Adv. Photonics Res.* **2022**, *3*, 2100315. [CrossRef]
30. Kim, H.H.; Lee, Y.; Lee, Y.J.; Jeong, J.; Yi, Y.; Park, C.; Yim, S.-Y.; Angadi, B.; Ko, K.-J.; Kang, J.-W.; et al. Realization of excitation wavelength independent blue emission of ZnO quantum dots with intrinsic defects. *ACS Photonics* **2020**, *7*, 723–734. [CrossRef]
31. Srinatha, N.; Angadi, B.; Son, D.I.; Choi, W.K. Structural and optical studies on spin coated ZnO-graphene conjugated thin films. *AIP Conf. Proc.* **2018**, *1953*, 100042.
32. Sharma, S.; Chawla, S. Enhanced UV emission in ZnO/ZnS core shell nanoparticles prepared by epitaxial growth in solution. *Electron. Mater. Lett.* **2013**, *9*, 267–271. [CrossRef]
33. Luo, J.; Zhao, S.; Wu, P.; Zhang, K.; Peng, C.; Zheng, S. Synthesis and characterization of new Cd-doped ZnO/ZnS core-shell quantum dots with tunable and highly visible photoluminescence. *J. Mater. Chem. C* **2015**, *3*, 3391–3398. [CrossRef]
34. Borgohain, R.; Das, R.; Mondal, B.; Yordsri, V.; Thanachayanont, C.; Baruah, S. ZnO/ZnS Core-Shell Nanostructures for Low-Concentration NO_2 Sensing at Room Temperature. *IEEE Sens. J.* **2018**, *18*, 7203–7208. [CrossRef]
35. Zhang, W.; Wang, S.; Wang, Y.; Zhu, Z.; Gao, X.; Yang, J.; Zhang, H.X. ZnO@ZnS core/shell microrods with enhanced gas sensing properties. *RSC Adv.* **2015**, *5*, 2620–2629. [CrossRef]
36. Mun, Y.; Park, S.; Ko, H.; Lee, C.; Lee, S. NO_2 gas sensing properties of ZnO/ZnS core-shell nanowires. *J. Korean Phys. Soc.* **2013**, *63*, 1595–1600. [CrossRef]
37. Qi, G.; Zhang, L.; Yuan, Z. Improved H_2S gas sensing properties of ZnO nanorods decorated by a several nm ZnS thin layer. *Phys. Chem. Chem. Phys.* **2014**, *16*, 13434–13439. [CrossRef]

38. Park, S.; Kim, S.; Ko, H.; Lee, C. Light Assisted Room Temperature Ethanol Gas Sensing of ZnO–ZnS Nanowires. *J. Nanosci. Nanotechnol.* **2014**, *14*, 9025–9028. [CrossRef]
39. Park, S.; Kim, S.; Ko, H.; Lee, C. Light-enhanced gas sensing of ZnS-core/ZnO-shell nanowires at room temperature. *J. Electroceramics* **2014**, *33*, 75–81. [CrossRef]
40. Gao, P.; Wang, L.; Wang, Y.; Chen, Y.; Wang, X.; Zhang, G. Onepot hydrothermal synthesis of heterostructured ZnO/ZnS nanorod arrays with high ethanol sensing properties. *Chem. Eur. J.* **2012**, *18*, 4681–4686. [CrossRef]
41. Na, C.W.; Park, S.-Y.; Lee, J.-H. Punched ZnO nanobelt networks for highly sensitive gas sensors. *Sens. Actuators B Chem.* **2012**, *174*, 495–499. [CrossRef]
42. Yu, X.-L.; Ji, H.-M.; Wang, H.-L.; Sun, J.; Du, X.-W. Synthesis and sensing properties of ZnO/ZnS nanocages. *Nanoscale Res. Lett.* **2010**, *5*, 644. [CrossRef]
43. Yu, X.; Zhang, G.; Cao, H.; An, X.; Wang, Y.; Shu, Z.; An, X.; Hua, F. ZnO@ZnS hollow dumbbells–graphene composites as high-performance photocatalysts and alcohol sensors. *New J. Chem.* **2012**, *36*, 2593–2598. [CrossRef]
44. Reiss, P.; Protière, M.; Li, L. Core/Shell Semiconductor Nanocrystals. *Small* **2009**, *5*, 154–168. [CrossRef] [PubMed]
45. Manaia, E.B.; Kaminski, R.C.K.; Caetano, B.L.; Magnani, M.; Meneau, F.; Rochet, A.; Santilli, C.V.; Briois, V.; Bourgaux, C.; Chiavacci, L.A. The Critical Role of Thioacetamide Concentration in the Formation of ZnO/ZnS Heterostructures by Sol-Gel Process. *Nanomaterials* **2018**, *8*, 55. [CrossRef] [PubMed]
46. Kim, J.-S.; Kang, B.-H.; Jeong, H.-M.; Kim, S.-W.; Xu, B.; Kang, S.-W. Quantum dot light emitting diodes using size-controlled ZnO NPs. *Curr. Appl. Phys.* **2018**, *18*, 681–685. [CrossRef]
47. Son, D.; Kwon, B.; Park, D.; Seo, W.S.; Yi, Y.; Angadi, B.; Lee, C.L.; Choi, W.K. Emissive ZnO–graphene quantum dots for white-light-emitting diodes. *Nat. Nanotechnol.* **2012**, *7*, 465–471. [CrossRef] [PubMed]
48. Briois, V.; Giorgetti, C.; Baudelet, F.; Blanchandin, S.; Tokumoto, M.S.; Pulcinelli, S.H.; Santilli, C.V. Dynamical Study of ZnO Nanocrystal and Zn-HDS Layered Basic Zinc Acetate Formation from Sol-Gel Route. *J. Phys. Chem. C* **2007**, *111*, 3253. [CrossRef]
49. Spanhel, L. Colloidal ZnO nanostructures and functional coatings: A survey. *J Sol-Gel Sci Techn.* **2006**, *39*, 7. [CrossRef]
50. Segets, D.; Marczak, R.; Schäfer, S.; Paula, C.; Gnichwitz, J.-F.; Hirsch, A.; Peukert, W. Experimental and Theoretical Studies of the Colloidal Stability of Nanoparticles−A General Interpretation Based on Stability Maps. *ACS Nano* **2011**, *5*, 4658–4669. [CrossRef]
51. Shuai, X.M.; Shen, W.Z. A Facile Chemical Conversion Synthesis of ZnO/ZnS Core/Shell Nanorods and Diverse Metal Sulfide Nanotubes. *J. Phys. Chem. C* **2011**, *115*, 6415–6422. [CrossRef]
52. Hu, Y.; Qian, H.; Liu, Y.; Du, G.; Zhang, F.; Wangb, L.; Hu, X. A microwave-assisted rapid route to synthesize ZnO/ZnS core–shell nanostructures via controllable surface sulfidation of ZnO nanorods. *CrystEngComm* **2011**, *13*, 3438–3443. [CrossRef]
53. Wang, F.; Liu, J.; Wang, Z.; Lin, A.-J.; Luo, H.; Yu, X. Interfacial Heterostructure Phenomena of Highly Luminescent ZnS/ZnO Quantum Dots. *J. Electrochem. Soc.* **2011**, *158*, H30. [CrossRef]
54. West, A.R. *Solid State Chemistry and Its Applications*, 2nd ed.; John Wiley and Sons: Hoboken, NJ, USA, 1992; ISBN 978-1-119-94294-8.
55. Meulenkamp, E.A. Synthesis and Growth of ZnO Nanoparticles. *J. Phys. Chem. B* **1998**, *102*, 5566–5572. [CrossRef]
56. Mehta, S.K.; Kumar, S.; Chaudhary, S.; Bhasin, K.K.; Gradzielski, M. Evolution of ZnS Nanoparticles via Facile CTAB Aqueous Micellar Solution Route: A Study on Controlling Parameters. *Nanoscale Res. Lett.* **2009**, *4*, 17. [CrossRef] [PubMed]
57. Balayeva, N.O.; Mamiyev, Z.Q. Synthesis and studies of CdS and ZnS-PE/NBR modified thermoplastic elastomeric copolymer nanocomposite films. *Mater. Lett.* **2016**, *162*, 121–125. [CrossRef]
58. Mamiyev, Z.Q.; Balayeva, N.O. Optical and structural studies of ZnS nanoparticles synthesized via chemical in situ technique. *Chem. Phys. Lett.* **2016**, *646*, 69–74. [CrossRef]